molecular pharmaceutics

Article

pubs.acs.org/molecularpharmaceutics

# Modification of Crystallization Behavior in Drug/Polyethylene Glycol Solid Dispersions

Qing Zhu,[†] Michael T. Harris,*[,†] and Lynne S. Taylor*[,‡]

[†]School of Chemical Engineering and [‡]Department of Industrial and Physical Pharmacy, Purdue University, West Lafayette, Indiana 47907, United States

Supporting Information

**ABSTRACT:** The crystallization kinetics of various active pharmaceutical ingredient/polyethylene glycol (API/PEG) solid dispersions has been investigated using wide-angle X-ray diffraction (XRD) and Raman spectroscopy. APIs with different physicochemical properties and crystallization tendency were employed to form solid dispersions with PEG. The crystallization rate of benzocaine (BZC) in BZC/PEG (20/80 wt %) solid dispersions was decreased substantially in comparison to that of the pure API, while the PEG matrix did not affect the crystallization behavior of haloperidol (HLP). The induction time for crystallization of ibuprofen (IBP) and fenofibrate (FNB) in a PEG matrix was decreased relative to the induction times for pure IBP and FNB. For the latter systems, it appears that crystalline PEG acted as a favorable heterogeneous nucleation site. The crystallization behavior of PEG in the API/PEG systems was also affected to different extents, depending on the API studied. These results suggest that PEG can delay, promote or have no influence on the crystallization kinetics of different APIs, and that any effects on crystallization behavior should be investigated in order to be able to produce a solid dispersion with consistent properties.

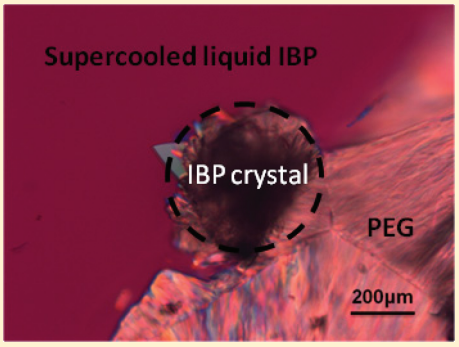


**KEYWORDS:** *crystallization, solid dispersions, kinetics, X-ray powder diffraction*

## INTRODUCTION

Solid dispersions of active pharmaceutical ingredients (APIs) in a biologically inert matrix have received extensive attention as a potential approach to increase the dissolution rate of poorly water-soluble APIs.[1−4] Most solid dispersions are prepared using highly water-soluble polymers as the carrier, where the polymer can be amorphous (e.g., polyvinylpyrrolidone (PVP)) or partially crystalline (e.g., polyethylene glycol (PEG)). Amorphous polymers are typically used to inhibit the crystallization of APIs and produce an amorphous dispersion.[2,3] For dispersions prepared with a semicrystalline polymeric carrier, the API can be amorphous, crystalline or semicrystalline, and the phase behavior of the system can be very complex.[1,3−7] It is important to understand the crystallization behavior of both the carrier and the API in these solid dispersions since it will affect the microstructure of the solid dispersion, and subsequently influence the dissolution behavior and bioavailability. It has been reported, for example, that nifedipine was present as a crystalline phase in a PEG dispersion,[8] whereas oxazepam was found to be amorphous in the PEG matrix.[9] It was also reported that the crystallization kinetics of PEG in lipid−PEG solid dispersions was governed by the properties of the lipid.[10] The majority of studies on API−PEG dispersions have focused on characterizing the final state of the API in PEG carrier; a comprehensive study of crystallization kinetics in semicrystalline polymer-based solid dispersions is lacking. However, the mutual crystallization behavior will influence the resultant dispersion microstructure and is consequently important to understand. It would be anticipated that PEG could either delay or promote crystallization of the API. Likewise, the API may influence the crystallization kinetics of PEG.

Given the importance of the crystallization process in determining the properties of the resultant solid dispersions, and the increasing interest in solid dispersions as drug delivery systems, the goal of the current research was to investigate the crystallization behavior of both the API and PEG in the dispersions. In our previous work, we studied the effect of the physicochemical properties of the API on the structural evolution of API−PEG solid dispersions. In these studies, it was found that the crystallization tendency of the pure API and the interaction between the API and PEG played important roles in determining the location of the API in the PEG matrix.[11,12] It is also of interest to understand how the physicochemical properties of the API will impact the crystallization behavior of the solid dispersions. The hypothesis to be tested in the current study is that the crystallization tendency of the pure API, combined with their ability to interact with the polymer, will impact the crystallization behavior of the APIs in the solid dispersions. In addition, the influence of the API on the crystallization of PEG is also of interest, since it has been reported that the

**Received:** August 2, 2011
**Revised:** January 6, 2012
**Accepted:** February 2, 2012
**Published:** February 2, 2012

spherulitic growth rate of PEG can be reduced upon addition of a second component that has favorable interaction with PEG.[13] Therefore, model APIs with different crystallization tendencies and interactions with PEG were selected for this study and dispersions were prepared by comelting with PEG. The crystallization kinetics was investigated using X-ray diffraction (XRD) and Raman spectroscopy.

## EXPERIMENTAL SECTION

**Materials and Sample Preparation.** Haloperidol (HLP) and fenofibrate (FNB) were obtained from Sigma-Aldrich Inc. (St. Louis, MO). Benzocaine (BZC) was purchased from Spectrum Chemical (Gardena, CA). Ibuprofen (IBP) was purchased from Albemarle Co. (Baton Rouge, LA). PEG with a molecular weight 3350 was a gift from The Dow Chemical Company (Midland, MI). Mixtures of the API and PEG were heated to above the melting temperature, and allowed to solidify at predetermined temperatures, of 25 or 40 °C. These crystallization temperatures were chosen to represent room temperature storage and a temperature intermediate to room temperature and the melting temperature of PEG. All samples were analyzed without further sample processing, and measures were taken to prevent the influence of atmospheric moisture (by either immediate sealing in the analysis chamber or storing in a desiccator over a desiccant in between measurements).

***In Situ* Synchrotron X-ray Diffraction (XRD).** Due to the extremely fast crystallization of PEG, time-resolved XRD experiments were conducted at the Advanced Photon Source beam station 5-ID-D, Argonne National Laboratory. The XRD instrument was equipped with a custom Roper charge-coupled detector. The energy of the X-ray source was 17 keV ($\lambda$ = 0.73 Å), and the distance of the sample to the XRD detector was 228 mm. The $q$ range for XRD was 0.6−4.6 Å$^{-1}$. The XRD range was calibrated using lanthanum hexaboride ($LaB_6$). Physical mixtures of the API and PEG were added to small aluminum pans (Tzero DSC sample pans, TA Instruments, New Castle, DE), and the aluminum pan was placed in a sealed Linkam DSC600 stage (Linkam Scientific Instruments Ltd., Surrey, U.K.) which was mounted in the X-ray beam. The samples were subjected to a temperature cycle using a Linkam CI-93 temperature programmer (Linkam Scientific Instruments Ltd., Surrey, U.K.). The sample was first heated to above the melting point of the API, followed by quench cooling to the specific solidification temperature. The time required for complete melting of the sample was determined by monitoring the XRPD pattern to ensure that all the diffraction peaks had disappeared.

**X-ray Diffraction (XRD).** Since the crystallization kinetics of certain APIs were much slower than others, and there was limited time available to use the Advanced Photon Source beam station 5-ID-D at the Argonne National Laboratory, XRD experiments were also conducted by using a Shimadzu XRD-6000 diffractometer (Shimadzu Corporation, Kyoto, Japan) Cu K$\alpha$ radiation ($\lambda$ = 1.54 Å). The voltage was 40 kV, and the current was 30 mA. The samples were scanned over a 2$\theta$ range of 4°−30°, with a step size of 0.04°, at a speed of 4° per min. To prepare the API/PEG solid dispersions, a physical mixture of API/PEG (20/80) was added to an aluminum sample holder, comelted by heating above the melting point for a sufficient length of time to ensure complete melting of all crystalline material, followed by cooling and solidification. The time required for complete melting was determined using hot stage microscopy experiments. Following preparation, samples were stored in a desiccator over phosphorus pentoxide and analyzed at different time intervals to monitor the crystallization kinetics of the API/PEG solid dispersions.

**Raman Spectroscopy.** The crystallization of the API in the API/PEG systems was also studied using a Kaiser RamanRXN2 Hybrid spectrometer (Kaiser Optical Systems, Inc., Ann Arbor, MI), equipped with a P$^h$AT-785 probe. The power was 400 mW, and the scan range was 1890−150 cm$^{-1}$. The spectrometer was controlled by icRaman 4.1 software. The API/PEG samples for the Raman spectroscopy studies were prepared and stored in an analogous manner as for the laboratory XRD studies.

**Cross-Polarized Optical Microscopy (CPOM).** To evaluate the crystallization behavior of either the pure API, pure PEG or the comelted API/PEG mixtures, samples were first melted on a hot plate on a glass coverslip and then placed in a sealed Linkam THMS 600 hot-stage (Linkam Scientific Instruments Ltd., Surrey, U.K.), held at either 25 or 40 °C. Samples were viewed using a Nikon Eclipse E600 polarized light microscope (Nikon Inc., Melville, NY).

## RESULTS AND DISCUSSION

**Crystallization Behavior of Pure APIs.** In order to understand the crystallization behavior of APIs in the PEG matrix, the crystallization behavior of pure HLP, BZC, IBP and FNB from the melt was studied using cross-polarized optical microscopy. The pure drugs were melted and then quench cooled to 25 °C. HLP and BZC crystallized before reaching the crystallization temperature, i.e. 25 °C, taking only a few seconds to completely crystallize. The crystallization was too fast for the kinetics to be captured. The induction time for crystallization of IBP and FNB was found to vary considerably between repeat samples reflecting the stochastic nature of nucleation. Therefore, following a similar approach to that developed by Jiang[14] for solution crystallization, the crystallization behavior of 50 samples was evaluated to conduct a statistical study of the induction time. $P(t)$ is the probability that IBP or FNB has started to crystallize at time $t$ when solidified at 25 °C. The $P(t)$ of IBP vs time is shown in Figure 1a. It shows that the probability of commencing crystallization within 1 h for IBP at 25 °C was 2/50 (i.e., 0.04), with the crystallization probability increasing to 10/50 (i.e., 0.2) after 3 weeks (504 h). For FNB (Figure 1b) the probability of commencing crystallization within 1 h was 4/50 (i.e., 0.08), and it increased to 17/50 (i.e., 0.34) after 3 weeks (Figure 1b). Figure 1 illustrates that the induction time probability is low over the time frame of hours/days and increases as the time frame is extended to weeks.

**Crystallization Kinetics of Pure PEG.** Due to the rapid crystallization kinetics of PEG, it is necessary to use an X-ray setup that allows for a rapid acquisition time. Hence, the crystallization of PEG at different temperatures was studied by *in situ* synchrotron XRD. Crystalline PEG has two main characteristic peaks at scattering vectors $q$ = 1.35 Å$^{-1}$ and 1.65 Å$^{-1}$, i.e. in terms of 2$\theta$ (when $\lambda$ = 1.54 Å) at 19.1° and 23.2° respectively. The apparent crystallinity of PEG, $\Phi_{peg}$, was determined from the ratio of the area under the PEG crystalline peaks to the overall area under the curve using a curve fitting program.[15] The percentage of crystalline material at time $t$, denoted as $X(t)$, is given by

$$X(t) = \Phi_{peg}(t)/\Phi_{peg}(\infty) \quad (1)$$

and was calculated by dividing the apparent crystallinity at time $t$ by the crystallinity when crystallization appears to be complete


dx.doi.org/10.1021/mp200546p | Mol. Pharmaceutics 2012, 9, 546−553

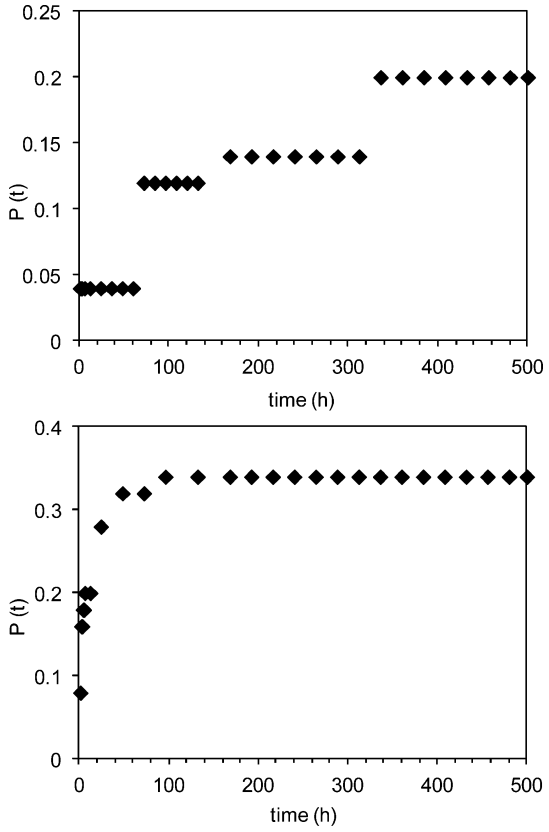


**Figure 1.** Induction time probability $P(t)$: (top) IBP crystallized at 25 °C; (bottom) FNB crystallized at 25 °C.

(i.e., where there is no further change in peak area). Figure 2 shows the percentage of crystalline material for PEG crystallized

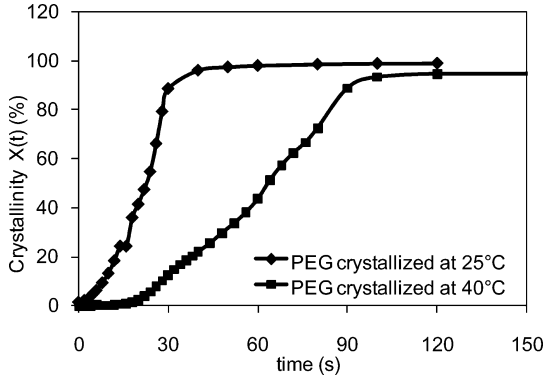


**Figure 2.** Crystallization kinetics of PEG at different temperatures based on synchrotron XRD results.

at different temperatures vs time. Here, time zero was taken as the time when PEG started to crystallize. It is apparent that PEG crystallized more slowly at 40 °C than at 25 °C, although it took less than 2 min for PEG to crystallize at both temperatures. The induction time for PEG crystallized at 25 °C is −10 s (i.e., the PEG commenced crystallization before 25 °C was reached), while that for PEG crystallized at 40 °C was 16 s.

The percent of crystalline material at time $t$, $X(t)$, was fitted to the Avrami model:[16−18]

$$X(t) = 1 - \exp(-zt^n) \quad (2)$$

where $z$ is a constant related to the crystallization conditions and $n$ is associated with the growth geometry of the crystal. If $n = 1$, it indicates linear growth of grains; $n = 2$, corresponds to platelike growth; $n = 3$ signifies polyhedral growth. The above statement is true with the assumption that nucleation is taking place at one instance. If nucleation occurs at a constant rate during crystallization, then $n$ becomes 2, 3, or 4 (one integer higher) respectively.[19] The fitted value of $n$ at both crystallization temperatures is less than 1. This suggested that the crystal growth tended to be one-dimensional, consistent with reports that the crystal growth is typically one-dimensional when growth is extremely fast.[20−22]

**Crystallization Kinetics in API/PEG Solid Dispersions.** In previous studies, the phase behavior of various API/PEG systems was evaluated[12,23] (for FNB/PEG systems, see Figure S1 in the Supporting Information). The various model APIs were found to have different estimated solubilities in supercooled liquid PEG, a range of interaction parameters, and crystallization tendencies. HLP was observed to have negligible solubility (less than 1% w/w) in PEG at 25 °C, while the solubility of BZC, IBP and FNB in PEG was estimated as 28%, 25% and 6% respectively using the binary phase diagrams[12,23] and Figure S1 in the Supporting Information and the Van't Hoff equation to extrapolate values to 25 °C.[11,12,24] Infrared studies suggested that HLP and FNB do not form hydrogen bonds with PEG, whereas BZC and IBP can interact with PEG through hydrogen bonding[12,23] (for FNB/PEG systems, see Figure S2 in the Supporting Information). Given the difference in drug−polymer interactions in the aforementioned systems, and previous reports that suggest that such differences can potentially impact crystallization behavior,[10,13,25] it is of interest to evaluate the crystallization behavior of the various API/PEG systems.

*HLP/PEG Systems.* For HLP/PEG (20/80) systems, the presence of PEG did not affect the crystallization kinetics of HLP. When the molten sample was cooled to 25 °C, HLP started to crystallize before PEG, and HLP crystallized completely within a few seconds. Due to the fast crystallization rate of HLP, the kinetics could not be captured by XRD. Figure 3

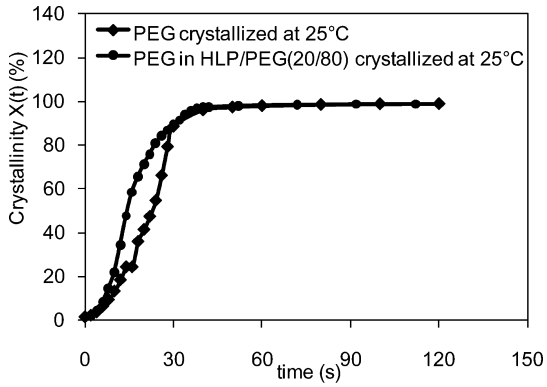


**Figure 3.** Crystallization kinetics of PEG in HLP/PEG (20/80) system crystallized at 25 °C based on synchrotron XRD data.

shows the crystallization kinetics of PEG in the HLP/PEG (20/80) system; crystallization of PEG commenced immediately after the crystallization of HLP, as seen from the synchrotron XRD data (not shown here). The crystallization kinetics for PEG solidified at 25 °C in the presence of the API were essentially the same as the crystallization kinetics of pure PEG at the same temperature.

*BZC/PEG Systems.* After loading 20% BZC in the PEG matrix, the induction time for the commencement of crystallization increased and the overall crystallization rate of BZC decreased substantially. BZC did not start to crystallize until after PEG had completely crystallized. BZC remained amorphous initially after the sample was cooled to 25 °C (see Figure 4). The induction period for the crystallization of BZC

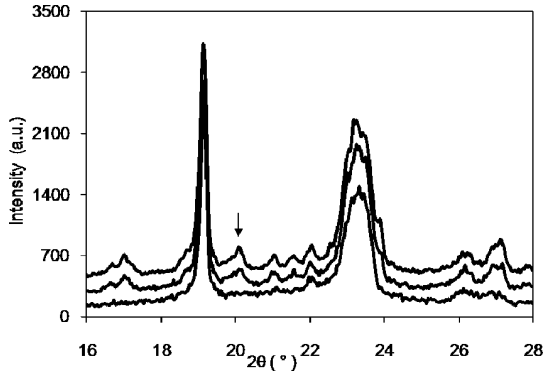


**Figure 4.** XRD of BZC/PEG (20/80) system crystallized at 25 °C for 30 min, 180 min and 300 min from bottom up (the arrow indicates the presence of crystalline BZC).

(based on the appearance of the characteristic diffraction peak at $2\theta$ = 20.1°) in the presence of 80% PEG is approximately 2−3 h.

The intensity of the BZC characteristics peaks in the XRD curves of the BZC/PEG dispersions was not sufficient for a kinetic study to be performed due to the relatively poor signal-to-noise ratio. Therefore, Raman spectroscopy was employed to study the crystallization kinetics (under similar experimental conditions to the XRD experiments) of the BZC in BZC/PEG (20/80) solid dispersions. Figure 5 shows the Raman spectra of

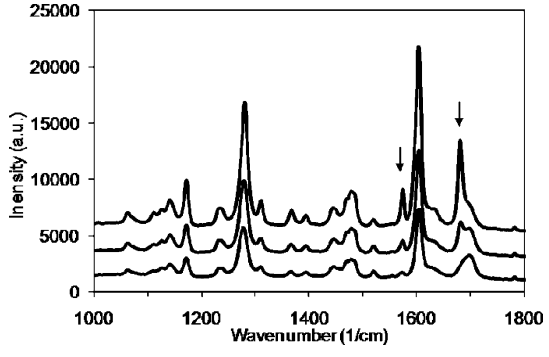


**Figure 5.** Raman spectra of BZC/PEG (20/80) system crystallized at 25 °C for 30 min, 180 min and 300 min from bottom up. The crystallization time from bottom to top: 30 min, 180 min and 300 min. (The arrows indicates the peaks used to generate the kinetic profile shown in Figure 6).

the BZC/PEG system when solidified at 25 °C. A new peak at 1680 $cm^{-1}$ appeared at 180 min (note the similar induction time to XRD experiments), and the intensity of the peak increased rapidly from 180 to 300 min. Similarly, the intensity of another peak at 1573 $cm^{-1}$ increased rapidly over approximately the same period. By comparing the spectra to the spectrum of crystalline BZC, these changes were found to be due to the crystallization of BZC in the BZC/PEG (20/80) solid dispersions. The change of the intensity of these two peaks as a function of time (time zero was taken as the point when the sample reached the predetermined solidification temperature, i.e. 25 °C) was plotted (Figure 6), yielding the kinetic profile

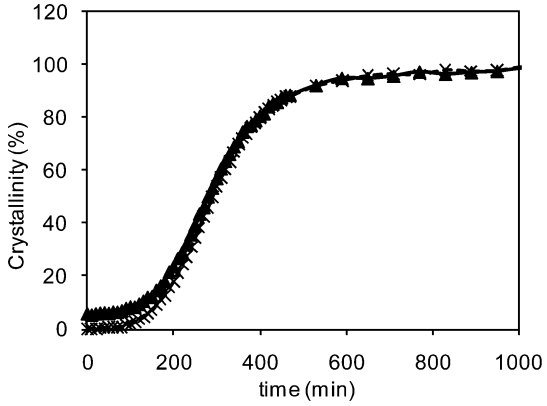


**Figure 6.** Crystallization kinetics of BZC in BZC/PEG (20/80) system crystallized at 25 °C (▲, based on Raman peak at 1573 $cm^{-1}$; ×, based on Raman peak at 1680 $cm^{-1}$).

for the crystallization of BZC in the solid dispersions. The crystallization kinetics based on the intensity of the peaks at 1573 $cm^{-1}$ and 1680 $cm^{-1}$ are extremely consistent. It took approximately 10 h to reach 90% relative crystallinity.

In addition to monitoring the crystallization kinetics of BZC in the solid dispersions, the crystallization kinetics of PEG in the BZC/PEG (20/80) solid dispersion was also studied using *in situ* synchrotron XRD. The crystallization rate of PEG in the dispersion was not significantly different from that of pure PEG (Figure 7) at the early stage of crystallization, while the crys-

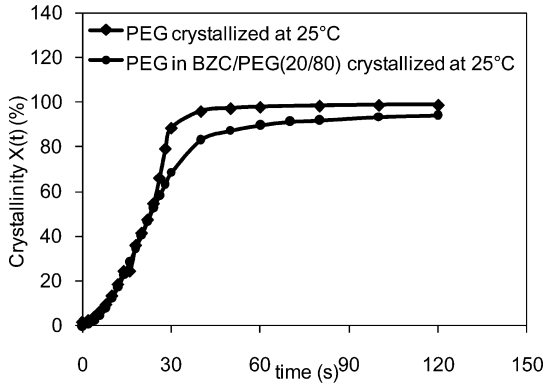


**Figure 7.** Crystallization kinetics of PEG in BZC/PEG (20/80) system crystallized at 25 °C based on synchrotron XRD data.

tallization rate of PEG at the later stage was reduced in the BZC/PEG system.

*IBP/PEG Systems.* Pure IBP was found to have a highly variable crystallization rate, either commencing crystallization in a few hours (lower probability) or staying amorphous for many days (higher probability), as summarized in Figure 1a. However, in the IBP/PEG (20/80) dispersion, synchrotron XRD studies indicated that IBP started to crystallize consistently within 2 h (indicated by the IBP crystalline peak at $2\theta$ = 20.2°), and completely crystallized within 4 h (Figure 8). The crystallization kinetics of IBP was also investigated using Raman spectroscopy. Two new peaks at wavenumber 746 $cm^{-1}$ and 784 $cm^{-1}$ appeared when IBP started to crystallize, and


dx.doi.org/10.1021/mp200546p | *Mol. Pharmaceutics* 2012, 9, 546−553

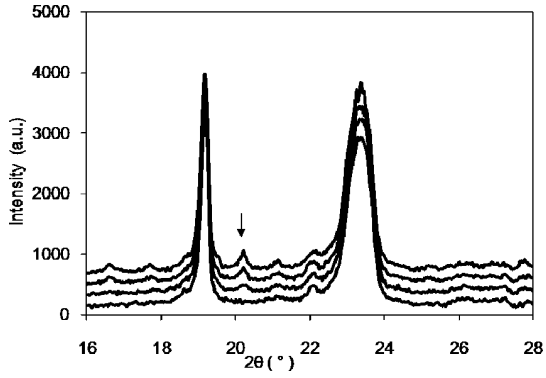


**Figure 8.** XRD of IBP/PEG (20/80) system crystallized at 25 °C for 20 min, 120 min, 150 min, and 220 min from bottom up (the arrow indicates the presence of crystalline IBP).

these peaks were used to study the crystallization kinetics of IBP in the solid dispersion (Figure 9). Figure 9 shows that the

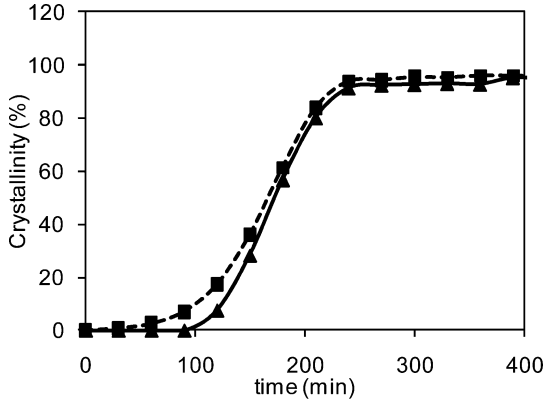


**Figure 9.** Crystallization kinetics of IBP in IBP/PEG (20/80) system crystallized at 25 °C (▲, based on Raman peak at 784 $cm^{-1}$; ■, based on Raman peak at 746 $cm^{-1}$).

induction time for the crystallization of IBP is approximately 100 min, and that IBP has crystallized to more than 90% relative crystallinity within 4 h. These results are consistent with the XRD data (Figure 8). The decrease in the average induction time for the crystallization of IBP in the dispersion was thought due to the additional heterogeneous nucleation sites provided by the crystalline PEG. To further confirm this hypothesis, a small piece of crystalline PEG was placed into supercooled liquid IBP at 25 °C, and the system was monitored by cross-polarized optical microscopy (Figure 10). From the image in Figure 10, it can be seen that crystallization of IBP has occurred (within the circle in Figure 10) at the interface between molten IBP and crystalline PEG (this occurred after a few minutes), while there were no nuclei visible in the bulk supercooled liquid IBP.

The crystallization rate of PEG in the IBP/PEG (20/80) dispersion at both 25 and 40 °C is shown in Figure 11 and compared to that of pure PEG. It is apparent that the crystallization rate of PEG in the IBP/PEG sample at 40 °C was much slower than the crystallization rate of pure PEG at the same temperature. The crystallization rates of PEG in the IBP/PEG samples and pure PEG were similar at 25 °C. The similar crystallization rates at 25 °C are probably due to the extremely fast crystallization of PEG at this temperature. Comparing Figures 9 and 11, it is apparent that the time frame

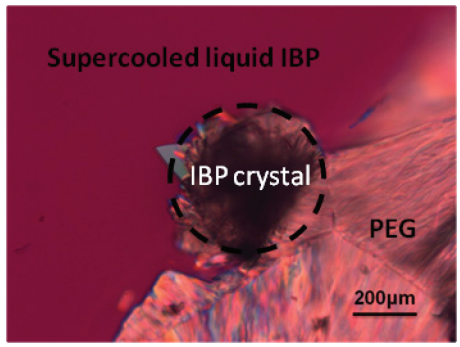


**Figure 10.** The formation of IBP crystal at the edge of the crystalline PEG particle at 25 °C.

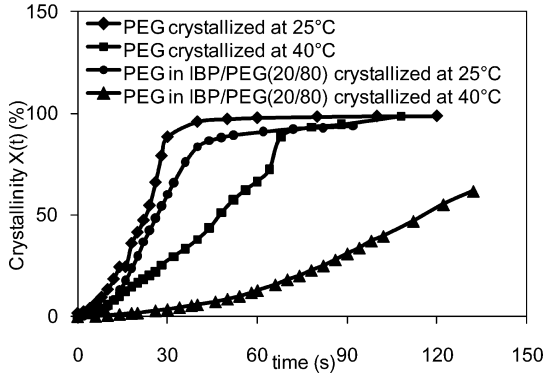


**Figure 11.** Crystallization kinetics of PEG in IBP/PEG (20/80) systems crystallized at different temperatures.

for PEG crystallization was much shorter than for IBP crystallization.

*FNB/PEG Systems.* The solidification of the FNB/PEG (20/80) dispersion was similar to that of the IBP/PEG system whereby PEG crystallized prior to FNB crystallization. The induction time for crystallization of FNB in the FNB/PEG system was also shorter than the induction time for the crystallization in pure FNB. On average, FNB started to crystallize after approximately 2−3 h in the dispersion, as indicated by the appearance of diffraction peaks at $2\theta$ = 16.2° and 16.8° (Figure 12). Raman spectroscopy revealed new peaks at 1648 $cm^{-1}$

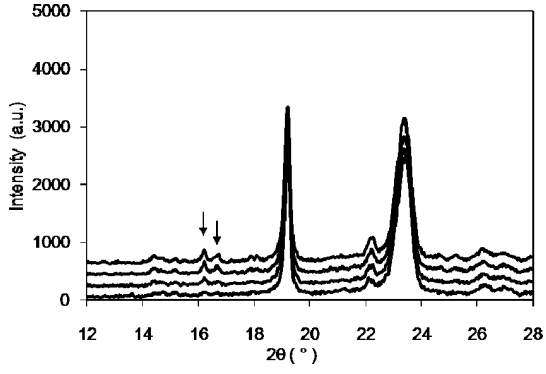


**Figure 12.** XRD of FNB/PEG (20/80) system crystallized at 25 °C for 180 min, 240 min, 380 min and 500 min for bottom up (arrows indicate the presence of crystalline FNB).

and 1419 $cm^{-1}$ during the crystallization of FNB. The crystallization kinetic data from the Raman spectroscopy analysis


dx.doi.org/10.1021/mp200546p | *Mol. Pharmaceutics* 2012, 9, 546−553

(Figure 13) demonstrated that it took approximately 9 h for FNB to achieve 90% relative crystallinity with a similar induction

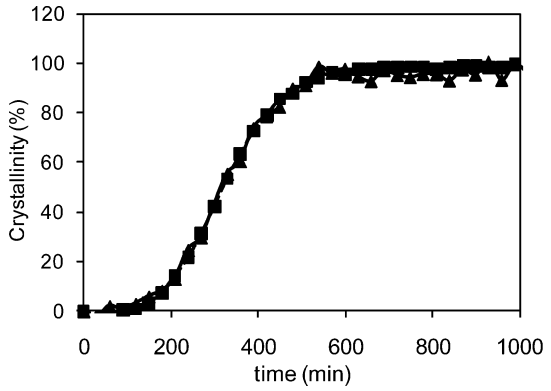


**Figure 13.** Crystallization kinetics of FNB in FNB/PEG (20/80) system crystallized at 25 °C (▲, based on Raman peak at 1419 $cm^{-1}$; ■, based on Raman peak at 1648 $cm^{-1}$).

time to that observed from the XRD experiments. The effect of crystalline PEG particles on the nucleation of FNB was likewise studied by placing a PEG particle into supercooled liquid FNB at 25 °C. Crystallization was observed immediately adjacent to the PEG particle within a few minutes (Figure 14), while no

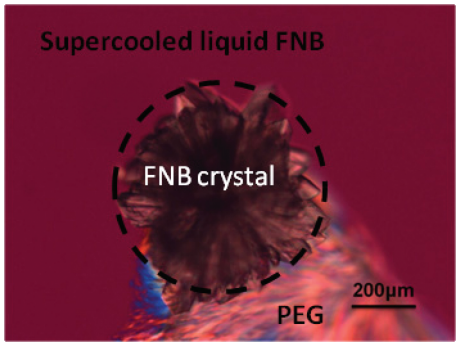


**Figure 14.** FNB crystal growth at the edge of the PEG particle crystallized at 25 °C.

crystallites were observed in the rest of the supercooled liquid. The crystallization kinetics of PEG in FNB/PEG systems was also studied (Figure 15). In the FNB/PEG systems, PEG

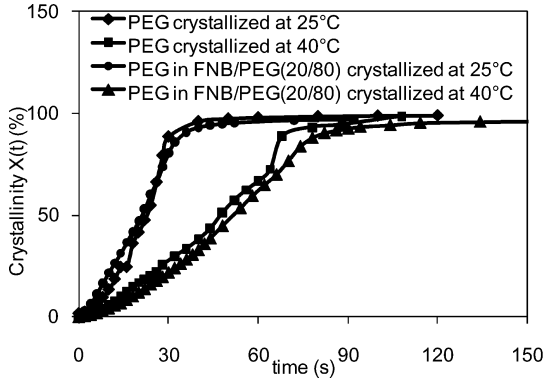


**Figure 15.** Crystallization kinetics of PEG in FNB/PEG (20/80) systems crystallized at different temperatures based on synchrotron XRD data.

crystallized much faster at 25 °C than at 40 °C. Interestingly, the crystallization kinetics of PEG in the FNB/PEG (20/80) system is very similar to that of pure PEG at the same crystallization temperatures.

**Growth Rate of PEG Spherulites in the Presence of Different APIs.** The growth rate of PEG spherulites in the absence and presence of various APIs (i.e., HLP, BZC, IBP and FNB) was also studied using cross-polarized optical microscopy. Since PEG grows too fast at 25 °C to obtain good kinetic data, the growth rate of the PEG spherulite was only studied at a crystallization temperature of 40 °C. Figure 16 shows the

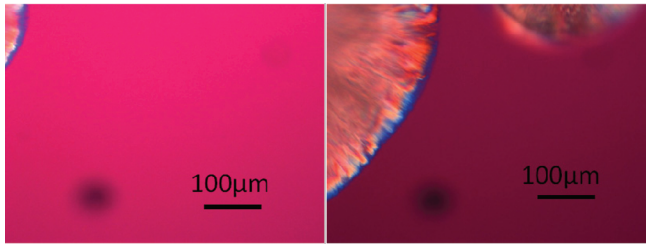


**Figure 16.** Growth of PEG spherulite at 40 °C: left image, 0 s; right image, 10 s.

growth of a PEG spherulite at 40 °C in pure PEG. The linear growth rate is 10 μm/s. Due to the large size of the spherulite, the whole spherulitic structure cannot be included in one single image. The linear growth rate of a PEG spherulite in the presence of various APIs is shown in Figure 17. The growth

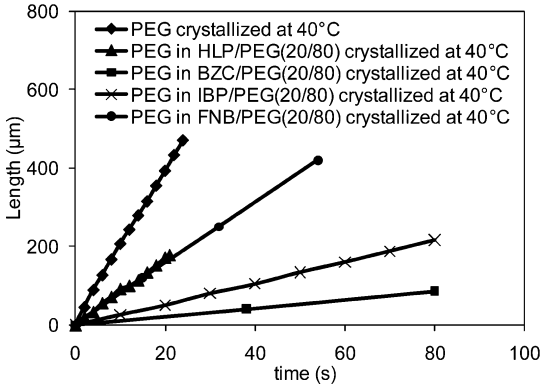


**Figure 17.** Linear growth of the PEG spherulite in various API/PEG systems at 40 °C.

rate of a PEG spherulite in HLP/PEG (20/80) or FNB/PEG (20/80) system (~8 μm/s) was slightly slower than that of pure PEG (~10 μm/s), while the growth rate of a PEG spherulite in IBP/PEG (20/80) or BZC/PEG (20/80) solid dispersions was much slower (3 μm/s and 1 μm/s, respectively) than that of pure PEG when crystallized at 40 °C.

Physicochemical properties of the API and PEG systems, induction time and time until 50% of the sample has crystallized ($t_{50}$) for the various API/PEG solid dispersions are summarized in Table 1. It can be seen that the crystallization rate of BZC in the BZC/PEG dispersion was much lower than the crystallization rate of pure BZC. The decrease of the crystallization rate is thought to be caused by the entropic mixing effects and favorable interactions formed between BZC and PEG which leads to substantial melting point depression of BZC in the presence of PEG. For a 20:80 dispersion, the


dx.doi.org/10.1021/mp200546p | Mol. Pharmaceutics 2012, 9, 546–553

Table 1. Summary of Various Properties and Crystallization Parameters for the API/PEG Systems[a]

| API | HLP | BZC | IBP | FNB |
|---|---|---|---|---|
| solubility of API in PEG at 25 °C (w/w)[11,12] | 0 | 28 | 25 | 6 |
| interaction of API with PEG through hydrogen bonding by FTIR[12,23] | no | yes | yes | no |
| $t_{ind}$ (API in API/PEG 20/80 system) | −100 s | 120−180 min | ∼100 min | 120−180 min |
| $t_{50}$[b] (API in API/PEG 20/80 system) | 7s | 110−170 min | ∼70 min | 140−200 min |
| $t_{ind}$ (PEG in API/PEG 20/80 system) | −12 s | 0 s | 8 s; 40 s (at 40 °C) | 1 s; 7 s (at 40 °C) |
| $t_{50}$[b] (PEG in API/PEG 20/80 system) | 15 s | 22 s | 26 s; 114 s (at 40 °C) | 21 s; 52 s (at 40 °C) |

[a]The crystallization temperature was 25 °C, unless otherwise stated. [b]The $t_{50}$ did not include the induction time.

concentration of BZC is below the eutectic composition, therefore, the melting point of BZC will be that of the eutectic, reported as around 48 °C.[12] This is considerably lower than the melting point of pure BZC[12] (around 89 °C), and hence the degree of supercooling at the solidification temperature is very different for the two systems. Pure BZC thus has a much larger thermodynamic driving force for crystallization relative to BZC in the BZC/PEG dispersion. The glass transition temperature of pure BZC is −31 °C,[26] and therefore the supposition that the difference in crystallization kinetics is caused by thermodynamic rather than kinetic factors is reasonable. In contrast to the BZC system, crystallization is promoted in IBP/PEG and FNB/PEG dispersions relative to the pure materials, and the induction time for the crystallization onset is reduced from a highly variable time period of hours to months, to approximately 100 min for IBP and 120−180 min for FNB. For both systems, a eutectic is formed with PEG, with IBP interacting more with PEG than FNB (based on the extent of the peak shift in the IR spectrum when mixing with PEG, see ref 12 and Figure S2 in the Supporting Information). The melting point depression for the IBP system is estimated to be about 30 °C,[12] while that for FNB is approximately 20 °C (see Figure S1 in the Supporting Information). Thus there is a reduced thermodynamic driving force for both systems that opposes crystallization. Despite this, the induction time is consistently reduced for both systems, suggesting that they nucleate more readily in the dispersion than for the pure drug. Based on the seeding studies reported in Figures 10 and 14, PEG appears to be able to promote heterogeneous nucleation by acting as a heterogeneous nucleation surface for both IBP and FNB. Indeed, several studies have demonstrated that polymers can act as heteronuclei for organic molecules, even influencing the polymorph that crystallizes,[27] although these studies investigated solution crystallization rather than melt crystallization as in our experiments. The observation that PEG promotes crystallization for some compounds is extremely interesting, since the majority of studies of drugs dispersed in polymers show the opposite effect, namely, that the polymer typically retards crystallization. The crystallization kinetics of the API in the formulation are extremely important from a bioavailability perspective; in order to achieve consistent delivery, the API should either be fully amorphous or fully crystalline at the time of administration, rather than containing a mixture of forms. Returning to the original hypothesis, the results of this study suggest that both the crystallization tendency of the drug and its ability to interact with PEG are of importance in influencing the crystallization kinetics of the components in the dispersion, with additional complicating factors coming into play for certain compounds where heterogeneous nucleation was promoted by PEG. Hence, if the crystallization tendency of the pure API is high (relative to that of pure PEG) and no favorable interactions occur between the API and PEG (exemplified by HLP), the PEG matrix has negligible effect on the crystallization kinetics of the API; if the crystallization of the pure API is fast but there are favorable interactions between the API and PEG (e.g., as for BZC), the onset of crystallization of API in the solid dispersions was observed to be delayed and the crystallization rate was reduced. Interestingly, the HLP:PEG system was the only monotectic system; the other systems were all eutectic systems with the concentrations employed in this study being close to the eutectic composition (for FNB/PEG systems, see Figure S1 in the Supporting Information).[12,23] The relationship between crystallization rate of the pure API and the API in the dispersion was found to break down for the slowly crystallizing compounds, IBP and FNB due to the apparent promotion of heterogeneous nucleation in these systems by PEG. Since it is well-known that particle size distributions are highly influenced by nucleation rates,[28−30] this could be an important factor that impacts the dissolution performance of solid dispersions.

It is also of interest to consider the influence of the APIs on the crystallization of PEG. The crystallization behavior of PEG in various API/PEG dispersions showed greater variation when crystallized at 40 °C, while negligible difference was observed at 25 °C. The crystallization of PEG in the IBP/PEG (20/80) system at 40 °C was slower than in pure PEG, while the crystallization rate of PEG in FNB/PEG system was almost the same as for pure PEG. The different behavior of PEG in the two systems is probably due to the differing ability of the two APIs to interact with PEG through hydrogen bonding.[13] IBP can form hydrogen bonds with PEG,[12] while FNB has limited ability to interact with PEG through hydrogen bonding since it lacks donor groups and PEG predominantly contains acceptor groups (see IR evidence for lack of interaction shown in Figure S2 in the Supporting Information). This is further confirmed by the study of the growth rate of PEG spherulites. In BZC/PEG and IBP/PEG systems (both APIs hydrogen bond with PEG[12]), the growth rate of PEG spherulites was slower than in the API/PEG systems where the API does not interact with PEG[23] (see Figure S2 in the Supporting Information). However, from a practical standpoint, PEG crystallization is still rapid in all systems (within a few minutes), although it is not known how changing the crystallization rate of PEG might influence the microstructure of the dispersion.

## ■ CONCLUSIONS

XRD, Raman spectroscopy and polarized light microscopy were used to compare the crystallization behavior of various APIs in the presence and absence of PEG. Depending on the specific API, the presence of PEG either accelerated the crystallization process, had no effect on the crystallization rate, or decreased the crystallization kinetics. Interestingly, PEG appeared to promote the heterogeneous nucleation of IBP and FNB,

accelerating the crystallization process in these two systems. The APIs were also found to influence the crystallization rate of PEG, although PEG was always observed to crystallize rapidly. These results are of practical and fundamental importance for the design of physically stable, consistently performing solid dispersions.

## ■ ASSOCIATED CONTENT

### Supporting Information

Phase diagram of FNB/PEG systems and infrared spectra of an FNB/PEG (20/80) mixture in the molten state. This material is available free of charge via the Internet at http://pubs.acs.org.

## ■ AUTHOR INFORMATION

### Corresponding Author

*M.T.H.: Purdue University, School of Chemical Engineering, 480 Stadium Mall Drive, West Lafayette, IN 47907; e-mail, mtharris@purdue.edu; tel, +1-765-494-8776; fax, +1- 765-494-0805. L.S.T.: Purdue University, Department of Industrial and Physical Pharmacy, 575 Stadium Mall Drive, West Lafayette, IN 47907; e-mail, lstaylor@purdue.edu; tel, +1-765-496-6614; fax, +1- 765-494-6545.

## ■ ACKNOWLEDGMENTS

Portions of this work were performed at the DuPont-Northwestern-Dow Collaborative Access Team (DND-CAT) located at Sector 5 of the Advanced Photon Source (APS). DND-CAT is supported by E.I. DuPont de Nemours & Co., The Dow Chemical Company and the State of Illinois. Use of the APS was supported by the U.S. Department of Energy, Office of Science, Office of Basic Energy Sciences, under Contract No. DE-AC02-06CH11357. We acknowledge the National Science Foundation Engineering Research Center for Structured Organic Particulate Systems (NSF ERC-SOPS) (EEC-0540855) for financial support.

## ■ REFERENCES

(1) Chiou, W. L.; Riegelman, S. Pharmaceutical Applications of Solid Dispersion Systems. *J. Pharm. Sci.* **1971**, *60* (9), 1281−1302.
(2) Leuner, C.; Dressman, J. Improving Drug Solubility for Oral Delivery Using Solid Dispersions. *Eur. J. Pharm. Biopharm.* **2000**, *50*, 47−60.
(3) Serajuddin, A. T. M. Solid Dispersion of Poorly Water-soluble Drugs: Early Promises, Subsequent Problems, and Recent Breakthroughs. *J. Pharm. Sci.* **1999**, *88*, 1058−1066.
(4) Craig, D. Q. M. The Mechanisms of Drug Release from Solid Dispersions in Water-Soluble Polymers. *Int. J. Pharm.* **2002**, *231*, 131−144.
(5) Craig, D. Q. M. Polyethylene Glycols and Drug Release. *Drug Dev. Ind. Pharm.* **1990**, *16* (17), 2501−2526.
(6) Lloyd, G. R.; Craig, D. Q. M.; Smith, A. An Investigation into the Melting Behavior of Binary Mixes and Solid Dispersions of Paracetamol and PEG 4000. *J. Pharm. Sci.* **1997**, *86* (9), 991−996.
(7) Lloyd, G. R.; Craig, D. Q. M.; Smith, A. An Investigation into the Production of Paracetamol Solid Dispersions in PEG 4000 Using Hot Stage Differential Interference Contrast Microscopy. *Int. J. Pharm.* **1997**, *158*, 39−46.
(8) Lin, C. W.; Cham, T. M. Effect of Particle Size on the Available Surface Area of Nifedipine from Nifedipine-Polyethylene Glycol 6000 Solid Dispersions. *Int. J. Pharm.* **1996**, *127*, 261−272.
(9) Ginés, J. M.; Arias, M. J.; Moyano, J. R.; Sánchez-Soto, P. J. Thermal Investigation of Crystallization of Polyethylene Glycols in Solid Dispersions Containing Oxazepam. *Int. J. Pharm.* **1996**, *143*, 247−253.
(10) Unga, J.; Matsson, P.; Mahlin, D. Understanding Polymer-Lipid Solid Dispersions − The Properties of Incorporated Lipids Govern the Crystallization Behavior of PEG. *Int. J. Pharm.* **2010**, *386*, 61−70.
(11) Zhu, Q.; Taylor, L. S.; Harris, M. T. Evaluation of the Microstructure of Semicrystalline Solid Dispersions. *Mol. Pharmaceutics* **2010**, *7* (4), 1291−1300.
(12) Zhu, Q.; Harris, M. T.; Taylor, L. S. Time-Resolved SAXS/WAXS Study of the Phase Behavior and Microstructural Evolution of Drug/PEG Solid Dispersions. *Mol. Pharmaceutics* **2011**, *8*, 932−939.
(13) Talibuddin, S.; Wu, L.; Runt, J. Microstructure of Melt-Miscible, Semicrystalline Polymer Blends. *Macromolecules* **1996**, *29*, 7527−7535.
(14) Jiang, S. F. *Crystallization Kinetics in Polymorphic Organic Compounds*, PhD dissertation, Delft University of Technology, ISBN 9789490122751, The Netherlands, 2009; p 133.
(15) Balta Calleja, F. J.; Vonk, C. G. *X-Ray Scattering of Synthetic Polymers*; Elsevier Science: New York, 1989; p 191.
(16) Avrami, M. Kinetics of Phase Change. I General Theory. *J. Chem. Phys.* **1939**, *7*, 1103−1112.
(17) Avrami, M. Kinetics of Phase Change. II Transformation−Time Relations for Random Distribution of Nuclei. *J. Chem. Phys.* **1940**, *8*, 212−224.
(18) Avrami, M. Granulation, Phase Change, and Microstructure. Kinetics of Phase Change. III. *J. Chem. Phys.* **1941**, *9*, 177−184.
(19) Mahlin, D.; Berggren, J.; Alderborn, G.; Engström, S. Moisture-Induced Surface Crystallization of Spray-Dried Amorphous Lactose Particles Studied by Atomic Force Microscopy. *J. Pharm. Sci.* **2004**, *93* (1), 29−37.
(20) Loo, Y. L.; Register, R. Polymer Crystallization in 25-nm Spheres. *Phys. Rev. Lett.* **2000**, *84* (18), 4120−4123.
(21) Mitchell, J. C.; Meier, D. J. Rapid Stress-Induced Crystallization in Natural Rubber. *J. Polym. Sci., Part A-2: Polym. Phys.* **1968**, *6*, 1689−1703.
(22) Blundell, D. J.; Mackerron, D. H.; Fuller, W.; Mahendrasingam, A.; Martin, C.; Oldman, R. J.; Rule, R. J.; Riekel, C. Characterization of Strain-Induced Crystallization of Poly(ethylene terephthalate) at Fast Draw Rates Using Synchrotron Radiation. *Polymer* **1996**, *37* (15), 3303−3311.
(23) Baird, J. A.; Taylor, L. S. Evaluation and Modeling of the Eutectic Composition of Various Drug-Polyethylene Glycol Solid Dispersions. *Pharm. Dev. Technol.* **2011**, *16* (3), 201−211.
(24) Connors, K. A. 2002. *Thermodynamics of Pharmaceutical Systems - An Introduction for Students of Pharmacy*; Wiley-Interscience: Hoboken, NJ, 2002; pp 118−119.
(25) Kestur, U. S.; Taylor, L. S. Role of Polymer Chemistry in Influencing Crystal Growth Rates from Amorphous Felodipine. *CrystEngComm* **2010**, *12*, 2390−2397.
(26) Baird, J. A.; Eerdenbrugh, B. V.; Taylor, L. S. A Classification System to Assess the Crystallization Tendency of Organic Molecules from Undercooled Melts. *J. Pharm. Sci.* **2010**, *99* (9), 3787−3806.
(27) Lang, M. D.; Grzesiak, A. L.; Matzger, A. J. The Use of Polymer Heteronuclei for Crystalline Polymorph Selection. *J. Am. Chem. Soc.* **2002**, *124*, 14834−14835.
(28) Mersmann, A. *Crystallization Technology Handbook*, 2nd ed.; Marcel Dekker, Inc.: New York, 2001; pp 145−184.
(29) Shevchenko, E. V.; Talapin, D. V.; Schnablegger, H.; Kornowski, A.; Festin, Ö.; Svedlindh, P.; Haase, M.; Weller, H. Study of Nucleation and Growth in the Organometallic Synthesis of Magnetic Alloy Nanocrystals: The Role of Nucleation Rate in Size Control of $CoPt_3$ Nanocrystals. *J. Am. Chem. Soc.* **2003**, *125*, 9090−9101.
(30) Byrappa, K.; Ohachi, T. *Crystal Growth Technology*; William Andrew Publishing: New York, 2003; p 326.